Model Predictive Control in the Multi-Megawatt Range

Thomas J. Besselmann, Sture Van de moortel, Stefan Almér, Pieder Jörg and Hans Joachim Ferreau

***Abstract*—The paper at hand presents an application of model predictive control to a variable speed drive system operating in the multi-megawatt range. The variable speed drive system comprises a synchronous machine fed by a line commutated rectifier and a load commutated inverter. The control task is to regulate the DC link current, and hence the machine torque, to ensure the machine speed follows a given reference. The proposed control approach is model predictive control where both the rectifier and inverter firing angles are considered as control inputs. The nonlinear model predictive torque controller has been implemented on an embedded system and applied in an industrial-scale pilot plant installation. The experiments show the successful operation of model predictive control on a plant with more than 48 MW power.**

***Index Terms*—Load commutated inverter, Predictive control, High-power application.**

I. Introduction

Model predictive control (MPC) [1], [2] is by now a standard solution in many applications with relatively slow system dynamics and ample computational resources. However, recent advances in optimization algorithms and computational hardware have enabled the use of MPC also in applications where sampling rates are higher and the controller is implemented on embedded platforms. In particular, MPC has been successfully applied for control of power converters and electric machines where the control frequency ranges from kilohertz to megahertz, see *e.g.*, [3]–[11].

The literature on MPC of power electronics is most often limited to either simulations or to laboratory-scale experimental setups. In contrast, the paper at hand reports an application of high-speed MPC to an *industrial-scale* pilot plant installation, with a variable-speed drive providing a gas compressor with power in excess of 48 MW.

The focus of most, if not all, previous research on MPC of power electronics has been on voltage source converter topologies. In the present paper we consider a synchronous machine fed by a load-commutated *current source* converter. To the best of our knowledge, MPC has not been applied to this type of system prior to the presented line of research.

Manuscript received May 22, 2015; revised September 10, 2015 and October 8, 2015; accepted November 1, 2015.

Corresponding author: T. Besselmann (phone: +41 58 586 74 40, e-mail: thomas.besselmann@ch.abb.com).

T. J. Besselmann, S. Almér and H. J. Ferreau are with ABB Corporate Research, Segelhofstrasse 1K, 5405 Baden-Dättwil, Aargau, Switzerland. S. Van de moortel and P. Jörg are with ABB Medium-Voltage Drives, Austrasse, 5300 Turgi, Aargau, Switzerland (e-mail:{thomas.besselmann, sture.vandemoortel, stefan.almer, pieder.joerg, joachim.ferreau}@ch.abb.com).

The paper considers a variable speed synchronous machine connected to the grid via a line commutated rectifier and a load commutated inverter (LCI) [12]. This type of variable speed solution is often the preferred choice in high power applications, ranging from a few megawatts to over a hundred megawatts, [13], [14]. Such applications include high speed compressors and rolling mills.

For the variable speed system at hand, we consider the design of a model predictive torque controller. The MPC considers both the rectifier and inverter firing angles as control inputs and minimizes the deviation of the DC link current from the reference while respecting constraints on the state and control inputs. By controlling the DC current, the machine torque is controlled indirectly to its reference.

The work presented here is motivated mainly by electrically-driven gas compression plants which are often situated in remote locations and operate under weak grid conditions. Weather phenomena occasionally produce sudden sags of the grid voltage, which can cause the drive to trip, interrupting or even aborting the gas compression process. The goal of this line of research is to design a more agile torque controller to increase the system robustness to external disturbances. In particular, we want to improve the ability to reliably ride through power loss situations due to grid faults and deliver torque during partial loss of grid voltage, [15].

Conventional PI-based control approaches typically assign different tasks to the two control inputs (*i.e.*, the rectifier and inverter firing angles). The inverter angle is set to determine the power factor of the machine, whereas the rectifier angle is used to control the DC link current. The fact that the MPC controls the rectifier and inverter angles without pre-assigning tasks to them implies a potential for better disturbance rejection. In particular, in the case of a disturbance of the grid, the PI approach would only adjust the rectifier angle while the MPC would adjust both firing angles.

Implementing the model predictive controller requires to solve a constrained nonlinear, nonconvex optimization problem in real-time. This is a challenging task as our application requires a sampling time of one millisecond and the embedded computing power is limited. Solving nonlinear MPC problems in such a situation requires both a careful problem formulation and highly efficient, state-of-the-art optimization algorithms. In this paper, we follow the promising approach of auto-generating customized nonlinear MPC algorithms that are tailored to the problem at hand based on a symbolic problem formulation as proposed in [16].

Preceding work in this line of research includes [17]. The paper at hand differs from the previous publication (a) in

(C) IEEE - DOI: 10.1109/TIE.2015.2504346

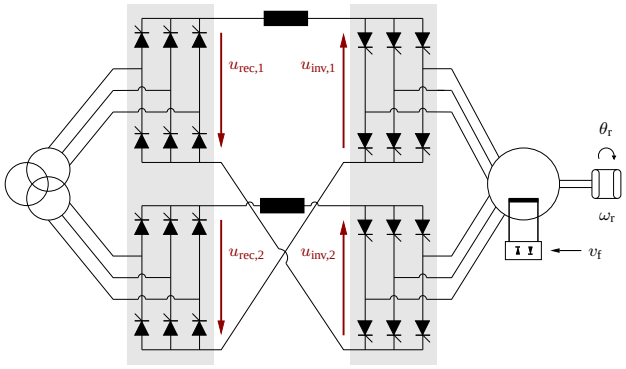

Fig. 1. Variable speed drive system comprised of line commutated rectifier, inductive DC link, load commutated inverter and synchronous machine.

its theoretical content by reformulating the torque control problem into a DC current control problem in order to simplify the optimization problem at hand; and (b) in its practical content by providing experimental data from tests on an industrial-scale pilot installation.

The paper is organized as follows. In Section II we describe the synchronous machine and the load-commutated inverter. Then a mathematical model of this system is presented in Section III. The developed control solution including the MPC current controller is described in Section IV. Section V contains the experimental results. Finally, conclusions are drawn in Section VI. Note that all quantities in this paper are normalized quantities.

II. Current Source Converters and Synchronous Machine

The paper considers a variable speed drive system composed of a line commutated rectifier, inductive DC link, load commutated inverter and a synchronous machine, see Fig. 1. This type of drive system is suitable for high power applications ranging from a few megawatts to over a hundred megawatts. Such applications include high speed compressors and rolling mills [18].

In the considered configuration the rectifier and inverter consist of twelve-pulse thyristor bridges, each comprising two six-pulse bridges. However, the proposed control scheme can easily be adapted to other configurations, such as six-pulse bridges and poly-phase synchronous machines as was considered in [17]. A thyristor bridge can operate as rectifier or as inverter, depending on the choice of the firing angle. In the context of this paper we will follow the common notation to denote the line side converter as rectifier and the machine side converter as inverter.

The control inputs (signals to be manipulated by the controller) are the firing angle α of the line side rectifier and firing angle β of the machine side inverter. Furthermore, the stator voltage magnitude u_{s} is controlled by means of an excitation voltage v_{f}. The variable to be controlled is the air gap torque produced by the synchronous machine.

III. Prediction Model

The model predictive controller is based on the dynamic model of the DC link and thyristor bridges developed below. The model describes the average behavior of the switched system. For the sake of simplicity, we neglect phenomena such as commutation overlap, thyristor recharge time, forced commutation at low speeds, asymmetric grid conditions, inductive voltage losses at the transformer or intermittent operation at low DC currents.

A. Control Input, State and Parameters

In deriving a dynamic model of the system suitable for torque control, we first decide which system quantities to model as states and which to consider as (slowly varying) parameters. Certain quantities are assumed to vary sufficiently slow to be approximated as constant when regulating the torque and are therefore considered as parameters. These quantities are the line voltage amplitude u_{l} and the machine voltage amplitude u_{s}. The state of the system consists of the DC link current i_{dc}.

The rotor excitation flux varies considerably slower than the DC link current i_{dc}. We therefore control the excitation of the machine with a slower outer loop and the design of this control loop is not discussed in this paper. The control variable (excitation voltage) v_{f} discussed above is therefore not considered in the sequel. Thus, the control input is the rectifier firing angle α and the inverter firing angle β.

B. DC Link Dynamics

The DC link current dynamics are described by

$$\frac{d}{dt}i_{\text{dc}} = \frac{1}{L_{\text{dc}}}\Big(- r_{\text{dc}} i_{\text{dc}} + u_{\text{rec},1} + u_{\text{rec},2} + u_{\text{inv},1} + u_{\text{inv},2} \Big),$$

where L_{dc}, r_{dc} are the inductance and parasitic resistance of the DC link inductor and where $u_{\text{rec},1}, u_{\text{rec},2}$ and $u_{\text{inv},1}, u_{\text{inv},2}$ are the DC voltage of each thyristor bridge of the rectifier and the inverter, respectively.

C. Thyristor Bridge DC Voltage

The DC side voltage of the six-pulse thyristor bridges in Fig. 1 is a switched waveform which is constructed by switching between the AC side line-to-line voltages. The principle is illustrated in Fig. 2 where the sinusoids represent the line-to-line voltages on the AC side and where the thick lines illustrate the DC side voltage for a few different values of the firing angle which ranges from 0 to 180 degree. The firing angle determines the time instant of the switch from one line-to-line voltage to another and this determines the average value of the DC side voltage. For a firing angle of 0 degree the thyristor bridge operates identical to a diode bridge, where the instant value of the line-to-line voltages determines which diodes are conducting. Larger firing angles represent the time delay of the thyristor bridge switchings compared to the switchings of a diode bridge.

For the purpose of control, we describe the average value of the switched DC side voltage as a function of the firing angle. The thyristor bridge DC voltage is approximated by a cosine of the firing angle as illustrated in Fig. 3. The approximation is intuitively clear considering the waveforms in Fig. 2. A derivation can be found in [19].

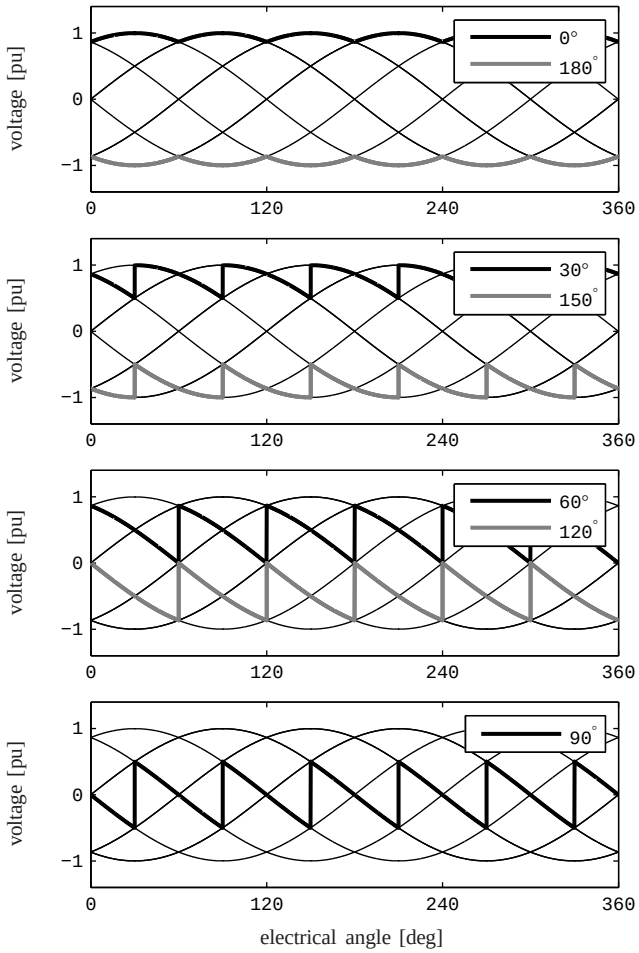

Fig. 2. AC and DC side voltages of a six-pulse thyristor bridge over one period of the AC side voltage. The thin lines show the line-to-line voltages on the AC side. The thick lines show the switched voltage of the DC side for different values of the firing angle.

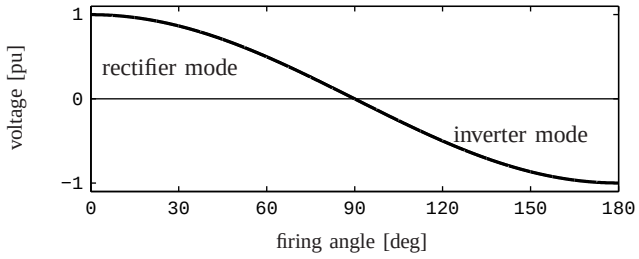

Fig. 3. DC side approximation: Approximate relation between AC and DC voltages of a thyristor bridge. The DC side voltage is approximated by a cosine of the firing angle.

By applying the same firing angle to both bridges of the converters and considering the sum of the DC side voltages, and by neglecting the switching and commutation intervals we have

$$u_{\text{rec}} \approx k_1 u_{\text{l}} \cos(\alpha), \quad u_{\text{inv}} \approx k_1 u_{\text{s}} \cos(\beta)\,,$$

where u_{rec} and u_{inv} are the combined DC side voltages of the line side and the machine side thyristor bridges, respectively, k_1 is a constant, u_{l} is the amplitude of the AC side voltage of the rectifier and u_{s} is the amplitude of the stator voltage, [20].

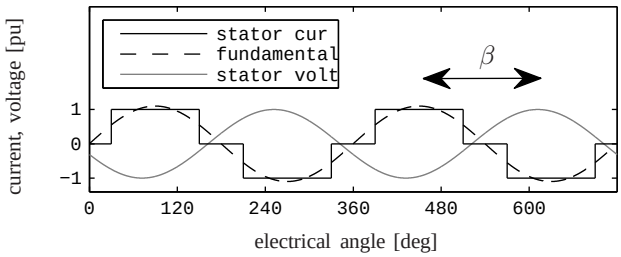

Fig. 4. AC side approximation: Stator current and its fundamental, and stator voltage of the synchronous machine. The power factor is determined by the angle β between current and voltage.

We note that the thyristors can be turned on at any time, but they can only be turned off by reducing the current running through them to zero. Thus, the off-switching of the thyristors is state dependent. This is neglected in the control model.

D. Thyristor Bridge AC Current

The AC side inverter current is illustrated in Fig. 4. The ideal waveform (neglecting commutation time [21]) is piecewise constant. For the purpose of control, the AC current is approximated by its fundamental component, which is illustrated by the dashed line in Fig. 4.

The modulator of the inverter, which takes the firing angle β and controls the switching, places the stator current at the angle β to the stator voltage and thus determines the power factor of the machine.

E. Torque Expression

The MPC problem formulation penalizes the deviation of the torque from a given reference and we therefore need an expression for the torque.

By scaling the nominal values accordingly, the electric power at the stator and the mechanical power at the shaft can be stated as

$$P_{\text{el}} = -u_{\text{s}} i_{\text{dc}} \cos(\beta), \qquad P_{\text{m}} = \tau_{\text{e}} \omega_{\text{r}}\,,$$

respectively. On average, and by ignoring the losses in the machine, the power balance holds, *i.e.* $P_{\text{m}} = P_{\text{el}}$, such that

$$\tau_{\text{e}} = -u_{\text{s}} i_{\text{dc}} \cos(\beta)/\omega_{\text{r}}.$$

Moreover, if the excitation controller adapts the excitation flux such that $u_{\text{s}} = \omega_{\text{r}}$, the torque expression simplifies to

$$\tau_{\text{e}} = -i_{\text{dc}} \cos(\beta).$$

F. Model Summary

By defining the line side and machine side power factors as auxiliary control variables $u_\alpha := \cos(\alpha)$ and $u_\beta := \cos(\beta)$, the prediction model can be stated as

$$\frac{d}{dt} i_{\text{dc}} = \frac{1}{L_{\text{dc}}} \left(-r_{\text{dc}} i_{\text{dc}} + u_{\text{l}} k_1 u_\alpha + u_{\text{s}} k_1 u_\beta\right)\,, \tag{1a}$$

$$\tau_{\text{e}} = -i_{\text{dc}} u_\beta\,, \tag{1b}$$

with the time-varying parameters u_{l} and u_{s}. By further replacing the torque as controlled variable by the current and the power factor, the prediction model simplifies to a one-dimensional linear parameter-varying system.

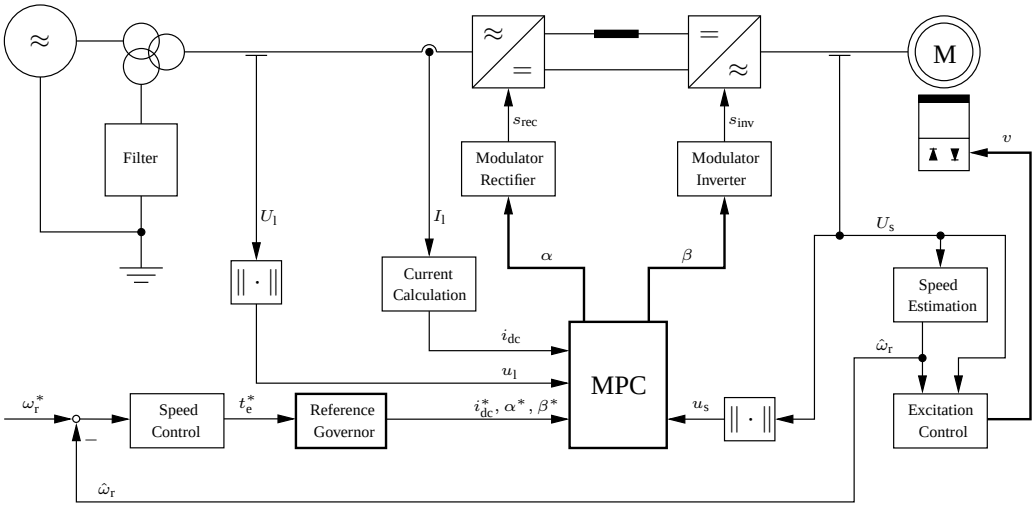

Fig. 5. Overview of the proposed control solution for load commutated inverter-fed synchronous machines.

IV. Proposed Control Solution

A simplified block diagram of the proposed control solution is shown in Fig. 5. Parts of the solution are state of the art and have been discussed in previous work, see *e.g.* [19], [22]. For brevity we thus focus on the innovative part of the control system, being the reference governor and the model predictive current controller.

A. Reference Governor

The task of the reference governor is to transform the torque reference τ_e^* into references i_dc^*, u_α^* and u_β^* for the DC current, the line side and the machine side power factor, respectively. Limitations on the eligible machine side firing angles,

$$\beta_\mathrm{min} \leq \beta \leq \beta_\mathrm{max}\,,$$

correspond to the auxiliary limitations

$$u_{\beta,\mathrm{min}} := \cos(\beta_\mathrm{max}) \leq u_\beta \leq \cos(\beta_\mathrm{min}) =: u_{\beta,\mathrm{max}}.$$

In order to minimize the reactive power in the machine, the power factor reference is set as large as possible, *i.e.*

$$u_\beta^* = \begin{cases} u_{\beta,\mathrm{min}}\,, & \text{if} \quad \tau_e^*\omega_\mathrm{r} \geq 0\,, \quad \text{(motoring)} \\ u_{\beta,\mathrm{max}}\,, & \text{if} \quad \tau_e^*\omega_\mathrm{r} < 0\,. \quad \text{(generating)} \end{cases}$$

Respecting some limitations on the permissible DC current

$$0 \leq i_\mathrm{dc} \leq i_\mathrm{dc,max}\,,$$

the DC current reference is chosen according to equation (1b) as

$$i_\mathrm{dc}^* = \begin{cases} i_\mathrm{dc,max}\,, & \text{if} \quad -\tau_e^*/u_\beta^* > i_\mathrm{dc,max}\,, \\ -\tau_e^*/u_\beta^*\,, & \text{if} \quad 0 \leq -\tau_e^*/u_\beta^* \leq i_\mathrm{dc,max}\,, \\ 0\,, & \text{if} \quad -\tau_e^*/u_\beta^* < 0\,. \end{cases}$$

Finally, a reference for the line side firing angle, α^* can be determined by means of the steady-state relation stemming from the prediction model (1a)

$$u_\alpha^* = \frac{1}{u_\mathrm{l} k_1}\left(r_\mathrm{dc} i_\mathrm{dc}^* - u_\mathrm{s} k_1 u_\beta^*\right)\,.$$

B. Model Predictive Current Controller

At each sampling time, the model predictive controller takes an estimate of the system state as initial condition and minimizes a finite time horizon cost integral subject to the dynamic constraints of the system and constraints on the state and input. The cost criterion is

$$J := \int_{kT_\mathrm{s}}^{kT_\mathrm{s}+T_\mathrm{p}} Q(i_\mathrm{dc} - i_\mathrm{dc}^*)^2 + \begin{bmatrix} u_\alpha - u_\alpha^* \\ u_\beta - u_\beta^* \end{bmatrix}^T R \begin{bmatrix} u_\alpha - u_\alpha^* \\ u_\beta - u_\beta^* \end{bmatrix} dt\,, \tag{2}$$

where k is the sampling instance, T_s is the sampling period and T_p is the prediction horizon length.

Model predictive control allows for the intuitive integration of constraints on inputs, states and outputs. In the application at hand we limit the eligible firing angles and request an upper bound on the DC current,

$$u_{\alpha,\mathrm{min}} \leq u_\alpha \leq u_{\alpha,\mathrm{max}}, \qquad u_{\beta,\mathrm{min}} \leq u_\beta \leq u_{\beta,\mathrm{max}}, \tag{3a}$$

$$i_\mathrm{dc} \leq i_\mathrm{dc,max}\,, \tag{3b}$$

for some application-dependent bounds. The time-continuous optimal control problem can thus be stated as

$$\min_{u_\alpha, u_\beta} (2) \quad \text{s.t.} \quad (1a), (3)\,. \tag{4}$$

In order to solve the optimal control problem (4) numerically, we follow a so-called "direct" approach (see e.g., [23] for a detailled discussion). This means that the optimal control problem is first discretized in time to yield a finite-dimensional nonlinear programming (NLP) problem, which can then be tackled by an appropriate optimization algorithm.

If the dynamic model would be linear, one would need to discretize problem (4) only once before the actual runtime of the controller. Moreover, in that case the resulting NLP would actually be a quadratic programming (QP) problem, such that the only computational effort to be performed on-line would be solving a (convex) QP problem. Recent years have seen a rapid development of on-line QP solvers that are able to solve such kind of linearized problems in the milli- or even microsecond range on embedded hardware, see *e.g.*, [24]–[28].

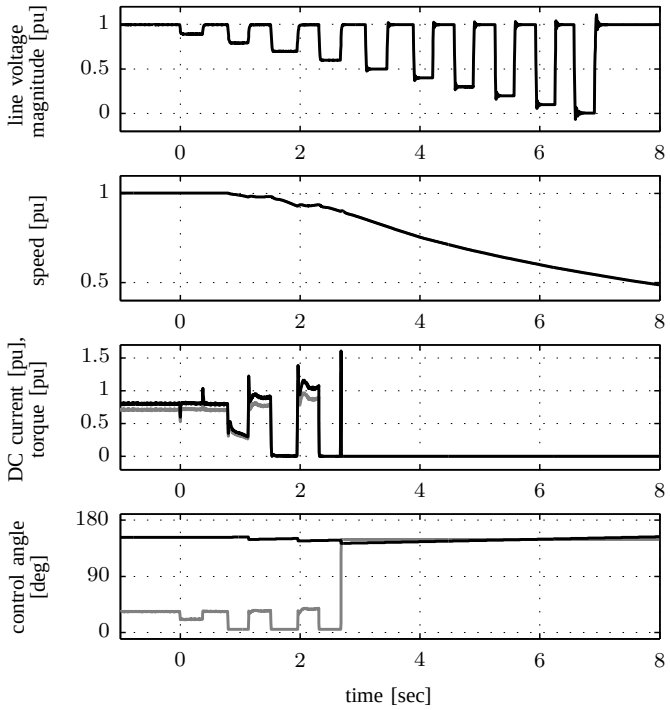

Fig. 6. Simulation results: Speed, DC current, torque and control angles during a voltage dip scenario with conventional PI control. The current and inverter angle are plotted in black. The torque and rectifier angle are plotted in gray.

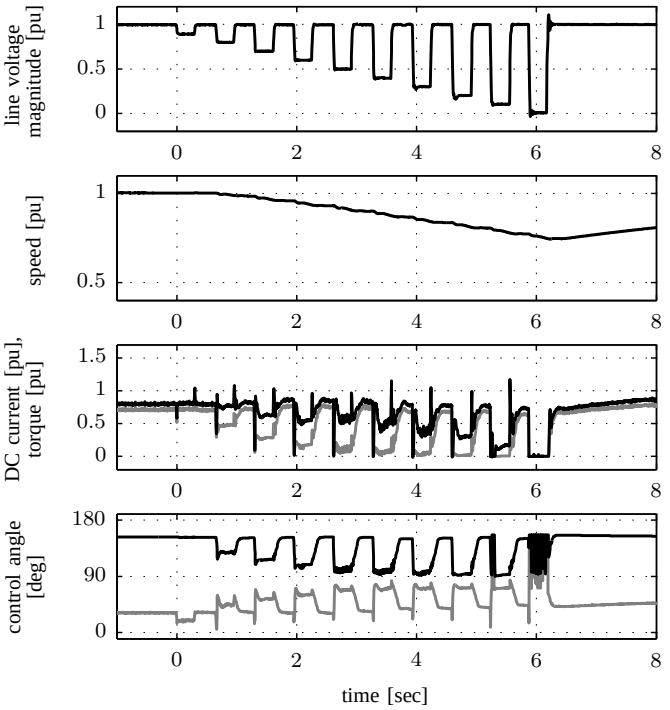

Fig. 7. Simulation results: Speed, DC current, torque and control angles during a voltage dip scenario with MPC. The current and inverter angle are plotted in black. The torque and rectifier angle are plotted in gray.

Since our system model is nonlinear, we are forced to perform the time-discretizaton of problem (4) on-line at each sampling instant. For doing so, cost criterion (2) is replaced by a finite sum over a fixed grid of discretization points, i.e.

$$J^{\text{disc}} := \sum_{j=0}^{N-1} Q(i_{\text{dc}}^j - i_{\text{dc}}^*)^2 + \begin{bmatrix} u_\alpha^j - u_\alpha^* \\ u_\beta^j - u_\beta^* \end{bmatrix}^T R \begin{bmatrix} u_\alpha^j - u_\alpha^* \\ u_\beta^j - u_\beta^* \end{bmatrix} + Q(i_{\text{dc}}^N - i_{\text{dc}}^*)^2 ,$$

where the superscript j (or N) denotes the respective quantity at time $t_j \in [kT_\text{s}, kT_\text{s}+T_\text{p}]$. Also the input and state bounds (3) are only imposed at these discretization points. Finally, time-discretization of the dynamic model (1a) is achieved by means of an on-line integrator (we applied an explicit Runge-Kutta scheme [29] with constant stepsize).

Along with this discretization in time, the integrator scheme also computes first-order derivatives of the state trajectory with respect to the initial state value and the control moves along the horizon (so-called sensitivities). We obtain a discrete-time *linearization* of the optimal control problem (4), which corresponds to a convex QP problem as in the case of linear dynamics. In order to reduce computational load for solving the resulting QP problem, we exploit its sparsity structure by eliminating all state variables from the QP formulation to arrive at a smaller-scale, dense QP problem. This QP problem is then solved by the on-line QP solver qpOASES [30], [31].

The procedure just described to solve nonlinear MPC problems is a sequential quadratic programming (SQP)-type approach known as real-time iteration scheme with Gauss-Newton approximation of the second-order derivatives [32]. In order to obtain a highly efficient implementation of this approach, we make use of the code generation functionality of the ACADO Toolkit [16]. This software takes a symbolic formulation of the control problem and allows the user to automatically generate customized nonlinear MPC algorithms that are tailored to the specific problem structure. The resulting C code is self-contained, highly optimized and able to run on embedded computing hardware.

In our case, the MPC algorithm was implemented on ABB's controller AC 800PEC, which is based on a 32-bit 600 MHz Power PC processor and which also includes an FPGA and a 64-bit floating point unit. The entire MPC solution, running with a sampling time of 1 ms, consumes only a minor fraction of the computational resources, such that the whole control system can be executed on time.

TABLE I
DESIGN DATA OF THE EXPERIMENTAL SYSTEM.

Parameter	Value	Unit
Line voltage, prim. side	132	kV
Line voltage, sec. side	7650	V
Line frequency	50	Hz
Rated line current, sec. side	2430	A
DC link inductance	5	mH
Rated DC current	2974	A
Rated stator voltage	6700	V
Rated stator current	2325	A
Rated stator frequency	58.33	Hz
Rated shaft power	48	MW
Rated rotational speed	3500	rpm

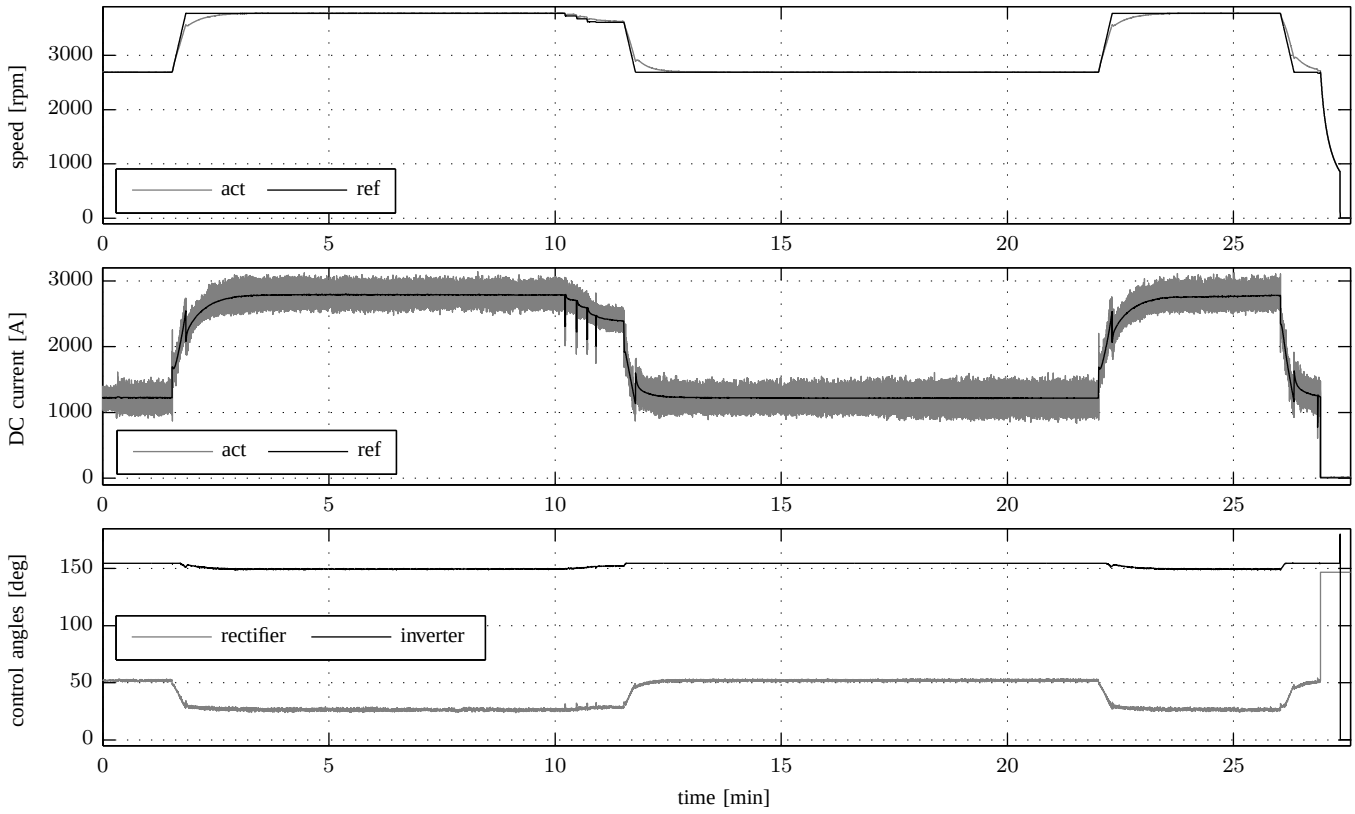

Fig. 8. Experimental results: Overview of recorded signals during experimental tests on an industrial-scale pilot plant installation.

V. Evaluation

The suggested model predictive current controller was applied to an industrial-scale pilot plant comprising ABB's Megadrive LCI, a dual-winding synchronous machine and a gas compressor. The two-pole synchronous machine has a nominal speed of 3600 rpm and a nominal power of 48 MW. The LCI is in a 12/12-pulse configuration as the one shown in Figure 1. The installation was connected via a transformer to the medium voltage grid with a grid voltage of 132 kV. For power factor correction and current harmonics compensation, electric filters are used. Table I summarizes the technical specifications of the setup.

A. HIL Simulations

Before applying the developed control solution to a medium voltage drive, it was tested in a hardware-in-the-loop (HIL) simulation environment. In the following the MPC scheme is compared to a conventional PI control approach in a scenario with heavy grid disturbances, where the system described above was simulated.

At the beginning of the scenario, the drive is operating with nominal speed. Then a sequence of instantaneous voltage dips of increasing magnitude occurs. Figures 6 and 7 show the selected control angles and the resulting DC link current during this scenario. The conventional PI controller is reacting only with the rectifier firing angle, which is not sufficient to sustain the DC link current (and thus the drive torque) during undervoltage conditions. Moreover there are big overshoots when the grid voltage returns, ultimately resulting in the activation of the overcurrent protection, and thus in tripping the drive.

In contrast the MPC solution: the constraint on the DC current (3) ensures that the height of the current peaks are limited and no trip occurs. Moreover, by actuating both control angles, the MPC is able to maintain the DC current and thus to provide some drive torque during undervoltage conditions. The amount of residual torque however is limited by the available grid voltage and by the tolerable height of the current peaks.

B. MV Drive Evaluation

After successful evaluation in HIL simulation, the MPC scheme was tested on a medium-voltage (MV) drive. An overview of the recorded signals is shown in Figure 8. The recorded signals are the speed reference ω_{r}^* and the actual speed ω_{r} of the rotor, the DC current reference i_{dc}^* provided by the reference governor and the actual DC link current i_{dc}, and the control angles α and β at the line side and the machine side of the converter.

In the top part of Figure 8, the speed reference ω_{r}^* and the actual speed ω_{r} of the rotor are displayed. The MPC is activated while the machinery is rotating with 2700 rpm. A number of speed reference ramps are requested, accelerating and decelerating the compressor between 2700 rpm and 3750 rpm. After around 27 minutes of operation, the drive is stopped and the compressor slows down to standstill.

The middle part of Figure 8 shows the DC current reference i_{dc}^* provided by the reference governor together with the actual

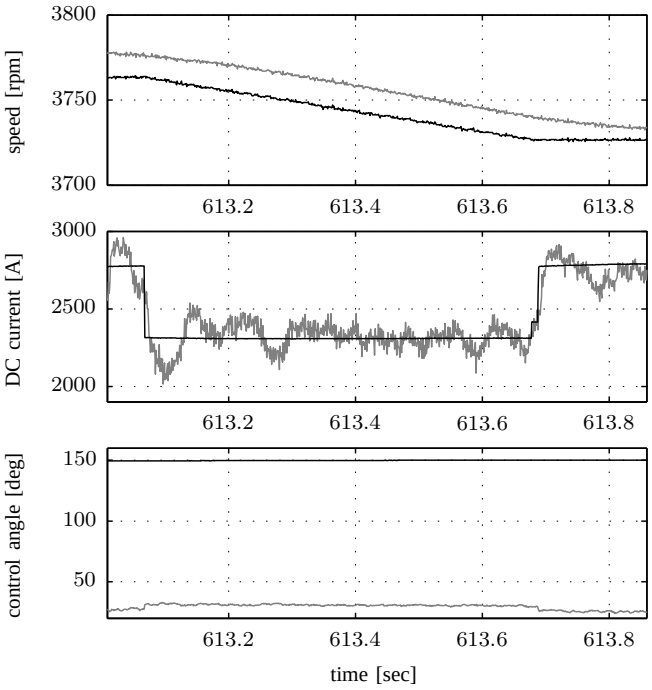

Fig. 9. Experimental results: Zoom to recorded signals at first speed decrease. For signal legend see Figure 8.

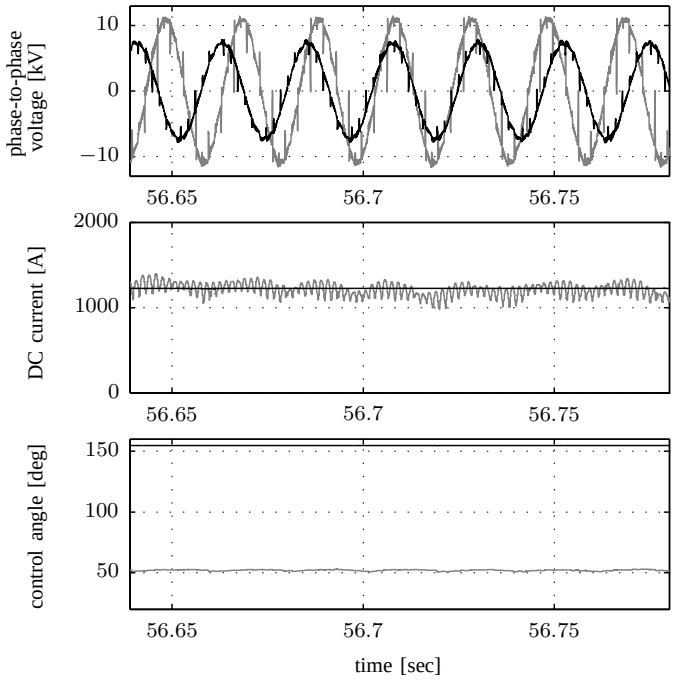

Fig. 10. Experimental results: Zoom to waveforms under steady-state conditions. Line side voltage plotted in gray, machine side voltage plotted in black. For remaining signal legend see Figure 8.

DC link current i_{dc}. It can be seen that at each speed reference ramp, the DC current reference exhibits step-wise changes. The actual DC current exhibits a large ripple. A certain amount of ripple is unavoidable, due to the topology of the load commutated inverter. A part of the DC current ripple is due to aggressive tuning of the MPC. The average of the DC current however is well-aligned with the DC current reference.

In the bottom part of Figure 8, the control angles α and β of the line side and the machine side of the converter are shown. With the suggested model predictive control solution, small deviations of the machine side control angle from a speed- and current-dependent upper bound $\beta_{\max}$ are taking place to support the regulation of the DC current. The line side firing angle α shows also a certain ripple for disturbance rejection.

More insight into the shape of the signals is provided in Figure 9. Exemplarily a zoom at the first decrease of the reference speed is shown, which was requested shortly after 10 minutes of operation. It can be seen how the DC current follows the stepwise changes of the current reference. For such a step it is sufficient to adapt the line-side firing angle, whereas the machine-side angle stays virtually constant.

The waveforms of the DC current and the phase-to-phase voltages under steady-state conditions are shown in Figure 10.

VI. Conclusion

The paper considered nonlinear model predictive control for torque regulation of a synchronous machine supplied by current source converters. By reformulating the torque control problem into a DC current control problem, a constrained control problem for a linear parameter-varying system is derived. In contrast to standard PI controllers, the MPC formulation does not impose a separate control structure, but uses both the rectifier and inverter angles simultaneously to stabilize the DC link current and thereby to control the torque. This increases the ability to stabilize the system and reject disturbances. Experimental verification on an industrial-scale pilot plant demonstrate the viability of the approach.

References

[1] J. M. Maciejowski, *Predictive Control with Constraints*. Prentice Hall, 2001.

[2] J. Rawlings and D. Mayne, *Model Predictive Control: Theory and Design*. Nob Hill Pub., 2009.

[3] S. Kouro, P. Cortes, R. Vargas, U. Ammann, and J. Rodriguez, "Model Predictive Control - A Simple and Powerful Method to Control Power Converters," *IEEE Trans. Ind. Electron.*, vol. 56, no. 6, pp. 1826–1838, June 2009.

[4] S. Bolognani, S. Bolognani, L. Peretti, and M. Zigliotto, "Design and Implementation of Model Predictive Control for Electrical Motor Drives," *IEEE Trans. Ind. Electron.*, vol. 56, no. 6, pp. 1925–1936, June 2009.

[5] S. Mariéthoz, A. Domahidi, and M. Morari, "High-Bandwidth Explicit Model Predictive Control of Electrical Drives," *IEEE Trans. Ind. Appl.*, vol. 48, no. 6, pp. 1980–1992, Nov. 2012.

[6] J. Scoltock, T. Geyer, and U. Madawala, "Model Predictive Direct Power Control for Grid-Connected NPC Converters," *IEEE Trans. Ind. Electron.*, vol. 62, no. 9, pp. 5319–5328, Sept. 2015.

[7] T. Geyer, G. Papafotiou, and M. Morari, "Model Predictive Direct Torque Control - Part I: Concept, Algorithm, and Analysis," *IEEE Trans. Ind. Electron.*, vol. 56, no. 6, pp. 1894–1905, June 2009.

[8] L. Tarisciotti, P. Zanchetta, A. Watson, S. Bifaretti, and J. Clare, "Modulated Model Predictive Control for a Seven-Level Cascaded H-Bridge Back-to-Back Converter," *IEEE Trans. Ind. Electron.*, vol. 61, no. 10, pp. 5375–5383, Oct. 2014.

[9] S. Almér, S. Mariéthoz, and M. Morari, "Sampled Data Model Predictive Control of a Voltage Source Inverter for Reduced Harmonic Distortion," *IEEE Trans. Control Syst. Technol.*, vol. 21, no. 5, pp. 1907–1915, Sept. 2013.

[10] Y. Xie, R. Ghaemi, J. Sun, and J. Freudenberg, "Model Predictive Control for a Full Bridge DC/DC Converter," *IEEE Trans. Control Syst. Technol.*, vol. 20, no. 1, pp. 164–172, Jan. 2012.
[11] S. Almér, S. Mariéthoz, and M. Morari, "Dynamic Phasor Model Predictive Control of Switched Mode Power Converters," *IEEE Trans. Control Syst. Technol.*, vol. 23, no. 1, pp. 349–356, Jan. 2015.
[12] A. B. Plunkett and F. G. Turnbull, "Load Commutated Inverter Synchronous Motor Drive Without a Shaft Position Sensor," *IEEE Trans. Ind. Electron.*, vol. IA-15, pp. 63–71, 1979.
[13] E. Wiechmann, P. Aqueveque, R. Burgos, and J. Rodriguez, "On the Efficiency of Voltage Source and Current Source Inverters for High-Power Drives," *IEEE Trans. Ind. Electron.*, vol. 55, pp. 1771–1782, Apr. 2008.
[14] R. Bhatia, H. Krattiger, A. Bonanini, D. Schafer, J. Inge, and G. Sydnor, "Adjustable speed drive with a single 100-MW synchronous motor," *ABB Review*, vol. 6, pp. 14–20, 1998.
[15] T. Wymann and P. Jörg, "Power loss ride-through in a variable speed drive system," in *Petroleum and Chemical Ind. Committee Europe (PCIC)*, June 2014, pp. 1–9.
[16] B. Houska, H. Ferreau, and M. Diehl, "An Auto-Generated Real-Time Iteration Algorithm for Nonlinear MPC in the Microsecond Range," *Automatica*, vol. 47, no. 10, pp. 2279–2285, 2011.
[17] S. Almér, T. Besselmann, and J. Ferreau, "Nonlinear model predictive torque control of a load commutated inverter and synchronous machine," in *Int. Power Electron. Conf., ECCE-ASIA*, Hiroshima, Japan, May 2014, pp. 3563–3567.
[18] A. Cortinovis, D. Pareschi, M. Mercangoez, and T. Besselmann, "Model predictive anti-surge control of centrifugal compressors with variable-speed drives," *Proc. 2012 IFAC Workshop on Automat. Control in Offshore Oil and Gas Prod.*, pp. 251–256, 2012.
[19] D. Schröder, *Elektrische Antriebe - Regelung von Antriebssystemen*, 3rd ed. Berlin; Heidelberg: Springer Verlag, 2009.
[20] BBC AG, *Silizium Stromrichter Handbuch*. Baden, Mannheim: BBC, 1971.
[21] R. S. Colby, T. A. Lipo, and D. W. Novotny, "A State Space Analysis of LCI Fed Synchronous Motor Drives in the Steady State," *IEEE Trans. Ind. Appl.*, vol. IA-21, no. 4, pp. 1016–1022, July 1985.
[22] W. Leonhard, *Control of Electrical Drives*. Berlin; Heidelberg; New York: Springer-Verlag, 2001.
[23] M. Diehl, H. J. Ferreau, and N. Haverbeke, *Nonlinear model predictive control*, ser. Lecture Notes in Control and Information Sciences. Springer, 2009, vol. 384, ch. Efficient Numerical Methods for Nonlinear MPC and Moving Horizon Estimation, pp. 391–417.
[24] H. J. Ferreau, H. G. Bock, and M. Diehl, "An online active set strategy to overcome the limitations of explicit MPC," *Int. J. Robust and Nonlinear Control*, vol. 18, no. 8, pp. 816–830, 2008.
[25] J. Mattingley and S. Boyd, *Convex Optimization in Signal Processing and Communications*. Cambridge University Press, 2009, ch. Automatic Code Generation for Real-Time Convex Optimization.
[26] S. Richter, S. Mariéthoz, and M. Morari, "High-Speed Online MPC Based on a Fast Gradient Method Applied to Power Converter Control," in *Proc. Amer. Control Conf. (ACC)*,, 2010, pp. 4737–4743.
[27] M.-A. Boéchat, J. Liu, H. Peyrl, A. Zanarini, and T. Besselmann, "An architecture for solving quadratic programs with the fast gradient method on a field programmable gate array," in *Mediterranean Conf. on Control Automat. (MED)*,, June 2013, pp. 1557–1562.
[28] H. Peyrl, A. Zanarini, T. Besselmann, J. Liu, and M.-A. Boéchat, "Parallel implementations of the fast gradient method for high-speed MPC," *Control Eng. Practice*, vol. 33, no. 0, pp. 22–34, 2014.
[29] E. Hairer, S. Nørsett, and G. Wanner, *Solving Ordinary Differential Equations I*, 2nd ed., ser. Springer Series in Computational Mathematics. Berlin: Springer, 1993.
[30] H. Ferreau, C. Kirches, A. Potschka, H. Bock, and M. Diehl, "qpOASES: A parametric active-set algorithm for quadratic programming," *Math. Programming Comput.*, vol. 6, no. 4, pp. 327–363, 2014.
[31] H. Ferreau, A. Potschka, and C. Kirches, "qpOASES webpage," http://www.qpOASES.org/, 2007–2015.
[32] M. Diehl, H. Bock, J. Schlöder, R. Findeisen, Z. Nagy, and F. Allgöwer, "Real-time optimization and Nonlinear Model Predictive Control of Processes governed by differential-algebraic equations," *J. Process Control*, vol. 12, no. 4, pp. 577–585, 2002.

Thomas J. Besselmann received his B.Sc. degree in general engineering science in 2003 and his Dipl.-Ing. degree in mechatronics in 2005 from Hamburg University of Technology, Germany. In 2010 he obtained his Ph.D. degree at the Automatic Control Laboratory, ETH Zurich, Switzerland. Currently he is employed as senior scientist in the Control & Optimization group at ABB Corporate Research, Switzerland. His research interests include high-speed control methods for constrained systems, in particular model predictive control, and their application to automotive and power electronics systems.

Sture Van de moortel graduated from the University of Applied Science in Lucerne in 2006 with a Dipl.-Ing. degree in electrical engineering. In 2007, he started his professional career at ABB Medium Voltage Drives and held different positions over the past years. His focus has been on LCI control and application software until he recently joined a Drive System Expert team focusing on large VSD systems, rotor dynamics, advanced regulation and interdisciplinary collaboration with our partners from industry.

Stefan Almér was born in Stockholm, Sweden. He received the M.Sc. degree in Engineering Physics in 2003 and the Ph.D. degree in Optimization and Systems Theory in 2008, both from the Royal Institute of Technology (KTH), Stockholm. Between 2008 and 2012 he held a research position at the Automatic Control Laboratory, ETH Zürich, Switzerland. Currently he is employed as senior scientist in the Control & Optimization group at ABB Corporate Research, Switzerland. His research interests include switched systems, model predictive control and control of power electronics.

Pieder Jörg received his M.Sc. degree 1995 from the Swiss Federal Institute of Technology, Zurich. He joined ABB at Corporate Research in the area of power electronics. In 2002 he joined the business unit Medium Voltage Drives as head of product development. Since 2010 he is focusing on business and technology development for demanding drives applications. He has been involved in various studies and improvement projects involving large VSD systems with demanding rotor dynamics.

Hans Joachim Ferreau studied mathematics and computer science at Heidelberg University, Germany, where he received a master degree in 2007. In 2011 he obtained a PhD degree in Electrical Engineering from KU Leuven, Belgium, with a doctoral thesis on numerical methods for fast model predictive control. In 2012 he joined ABB's corporate research center in Baden-Dättwil, Switzerland, where he currently works as senior scientist on various applications of optimization-based control. His current research is focussing on tools and algorithms for embedded optimization, such as model predictive control.